Influence of criteria on the determination of forming limits in thickness reduced cruciform specimens

Z Wang [1], D Guines [1] and L Leotoing [1]*

[1] Univ Rennes, INSA Rennes, LGCGM (Laboratoire de Génie Civil et Génie Mécanique) - EA 3913, F-35000 Rennes, France

* lionel.leotoing@insa-rennes.fr

Abstract. Biaxial tensile test methods using cruciform specimens have been drawing attention as an effective approach to characterize sheet metal formability. The cruciform specimens usually adopt a thickness reduction at the central area to achieve a relatively large strain gradient for localized necking and fracture investigation. For conventional tests, many criteria have been proposed to determine the forming limits at necking, however, none has been widely accepted and applied to the cruciform specimens with non-uniformed thickness reduction. Therefore, in this work, different existing necking criteria are applied and discussed for numerical procedure in order to define an appropriate necking criterion for the thickness reduced cruciform specimens. AA6061-T4 sheet with a thickness of 2mm is used as a target material. The predicted forming limit curves are compared for different criteria, and the feasibility of each criterion is discussed in detail. Thanks to two dedicated specimens proposed by the authors, forming limits are determined for a wide range of strain states.

1. Introduction

The forming limit curve (FLC) is the common tool for assessing the formability of sheet metals. It's represented in the space of principal major and minor strains and illustrates the limit strains at the onset of localized necking under various linear strain paths [1]. The two primary experimental methods recommended by the international standard ISO 12004-2 [2], the Nakazima and Marciniak tests, have been standardized to construct the FLC of sheet metals. Both tests use punches to form a set of specimens with varying widths to obtain limit strains under different strain paths. It's necessary to have a nearly frictionless state in the zone of evaluation, since friction can influence the position of necking and the linearity of the strain path [3]. Thus, the lubrication measures are commonly employed between the punch and specimen. However, expending the applications of the tests to determine the sheet metal formability at high temperatures remains a challenge, since the limited thermal stability of lubricants [4]. In recent years, biaxial tensile test with a dedicated cruciform specimen has become an interesting alternative to determine the FLC for sheet metals, especially at high temperatures and large strain rates. The test is frictionless and the strain path can be directly controlled by adjusting the biaxial tensile ratios [5].

Significant efforts have been made to design cruciform specimens for the sheet metal formability evaluation. A common feature of these cruciform specimens is the use of a progressive thickness reduction in the specimen central area, and the aim is to achieve a relatively large strain gradient for localized necking and fracture. For example, Zidane et al. [6] proposed a cruciform specimen with a two-step thickness reduction at the central area to determine the FLC of the AA5086 sheet. Song et al.

Content from this work may be used under the terms of the Creative Commons Attribution 3.0 licence. Any further distribution of this work must maintain attribution to the author(s) and the title of the work, journal citation and DOI.
Published under licence by IOP Publishing Ltd

[7] proposed a cruciform specimen with slits in each arm and progressive thickness reduction at central area to determine the FLC of the DP600 sheet. However, this kind of non-uniformed thickness reduction introduces uncertainty in determining the forming limits at necking, since almost all of the existing necking criteria are developed for flat specimens. Therefore, it's necessary to investigate the feasibility of the existing criteria in determining the forming limits based on the thickness reduced cruciform specimen.

The necking criteria can be classified into three categories: position-dependent method, time-dependent method and position-time-dependent method. As defined in ISO 12004-2, the position dependent method evaluates the distribution of the principal main strains along the cross section perpendicular to the crack, and the necking strain corresponds to the highest point of an inverse parabolic curve which is fitted to the main strains [8]. The time-dependent method is based on the evaluation of strain history. The forming limits at necking are determined at the moment of the abrupt change in the first or the second time derivative of strains [9]. For example, Iquilio et al. [10] proposed a necking detection method by means of thickness variation and applied it to determine the forming limits for AISI 430 stainless steel. In this method, the center and edge of the necking area were identified, and the onset of localized necking is considered as the moment when the thickness variation rate curve at the edge of necking area changes its slope drastically. For the position-time-dependent method, the basic concept is the analysis of the difference in the strain evolution between necking and the adjacent areas. The strain increment ratio method is a typical position-time-dependent method and is frequently adopted in the M-K model [11]. In this method, the localized necking is assumed to occur when strain increment ratio between a point located in the necking area and a point in the adjacent area reaches the critical value [12]. In addition, Zhang et al. [13] proposed a necking detection method by analyzing the evolutions of the average thickness strain for two rectangular zones, and applied it to determine the forming limits of AA5754 in the biaxial tensile test.

In this paper, four different necking criteria were applied to detect the forming limits in the numerical simulation of the in plane biaxial test. The predictions of all the criteria are discussed in order to recommend an appropriate necking criterion for the thickness reduced cruciform specimens. Two dedicated cruciform specimens were employed to cover the strain paths from equi-biaxial to uniaxial tension. Finite element (FE) simulations coupled with the Gurson–Tvergaard–Needleman (GTN) model were conducted to predict failure behaviours of AA6061 sheets.

2. FE model construction and FLC prediction

2.1. Numerical simulation of the biaxial tensile test

AA6061-T4 sheets with 2mm thickness were selected for the study. The FE models based on two dedicated cruciform specimens (shown in Figure 1) were built in ABAQUS/Explicit. By adjusting the biaxial tensile ratios between the L1 and L2 directions, Specimen I [7] was used to obtain the strain paths from equi-biaxial to plane strain, and specimen II [14] was used to obtain the strain paths from plane strain to uniaxial tension. The FE models were modeled by eight-node brick solid elements with reduced integration (C3D8R), and the element size was refined in the thickness reduced zone to ensure the accuracy of the predictions, with a minimum mesh size of 0.2mm. In addition, 3 elements were adopted in the thickness direction.

The basic mechanical properties of the AA6061-T4 sheet used in simulations were obtained from uniaxial tensile tests at room temperature and quasi-static strain rate ($0.002s^{-1}$) along rolling direction. The strain hardening of the material was described by the Voce hardening function, as shown in equation (1).

$$\sigma_{\text{Hard}} = \left[166.6 + 191.3 \times \left(1 - e^{-13.3 \cdot \bar{\varepsilon}^{p}}\right)\right] \text{MPa} \quad (1)$$

In order to consider the damage effects and to predict the failure behavior of the material, the GTN model [15] was employed and implemented in ABAQUS by the user subroutine VUMAT. The yield function of the GTN model takes the following form:

$$\Phi = \left(\frac{\sigma_e}{\sigma_{Hard}}\right)^2 + 2q_1 f^* \cosh\left(\frac{3q_2\sigma_m}{2\sigma_y}\right) - 1 - \left(q_1 f^*\right)^2 = 0 \tag{2}$$

$$f^* = \begin{cases} f & f \le f_c \\ f_c + \dfrac{f_u - f_c}{f_f - f_c}\left(f - f_c\right) & f > f_c \\ f_u & f = f_f \end{cases} \tag{3}$$

$$\dot{f} = \dot{f}_{grow} + \dot{f}_{nucl}; \quad \dot{f}_{grow} = (1-f)\dot{\boldsymbol{\varepsilon}}^P : \boldsymbol{I}; \quad \dot{f}_{nucl} = A_N \cdot \dot{\bar{\varepsilon}}^P \tag{4}$$

$$A_N = \frac{f_n}{S_n\sqrt{2\pi}} \exp\left(-\frac{1}{2}\left(\frac{\bar{\varepsilon}^P - \varepsilon_n}{S_n}\right)\right) \tag{5}$$

Where σ_{Hard} is the yield stress evolving with the material hardening, σ_e is the von Mises equivalent stress, $\sigma_m = \sigma_{ii}/3$ is the mean stress. q_1 and q_2 are material coefficients. f is the void volume fraction of the material and f^* is the effective void volume fraction. f_c is the void volume fraction to trigger coalescence, $f_u = 1/q_1$ is the ultimate volume fraction and f_f represents the void volume fraction at fracture. f_n represents the volume fraction of the nucleated void, ε_n is the mean value of the normal distribution of the nucleation strain, and S_n is the standard deviation. The main parameters in the GTN model are listed in Table 1 [16].

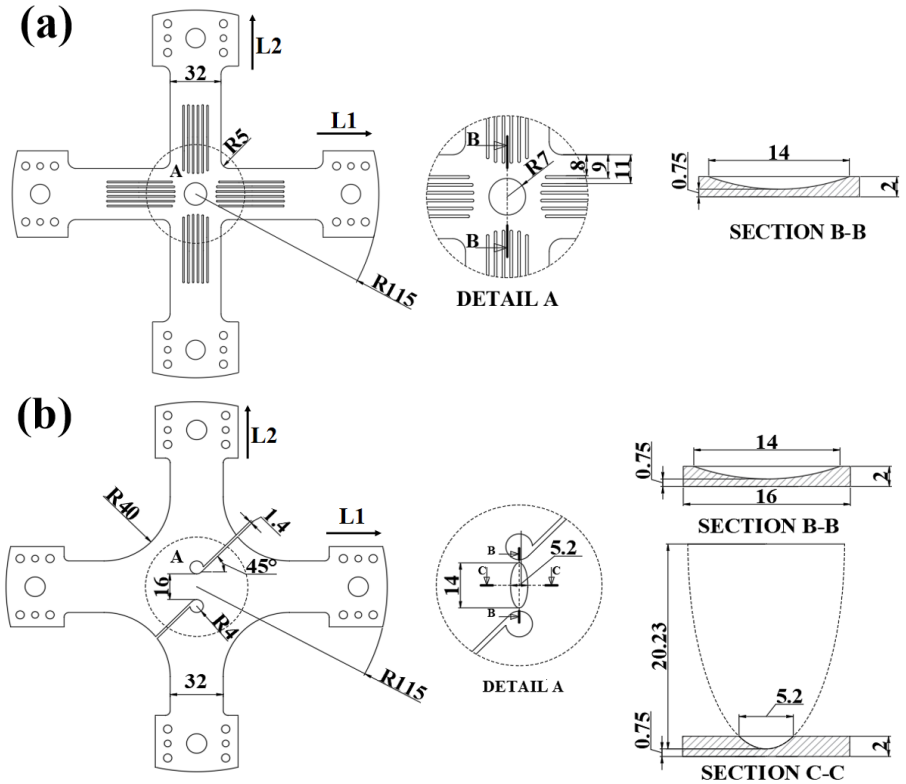


Figure 1. Dimensions of the used cruciform specimens (unit: mm): (a) Specimen I, (b) specimen II

Table 1. Main parameters in the GTN model

Parameters	q_1	q_2	f_n	S_n	ε_n	f_0	f_c	f_f
Value	1.5	1	0.01285	0.07	0.168	0.00025	0.01755	0.02887

2.2. FLC prediction with different necking criteria

2.2.1. Position dependent method (CRIT1). As the method is explicitly explained in ISO 12004-2 [2], a brief introduction is given here and the simulation results of specimen I under equi-biaxial loading condition are used as an example. As shown in Figure 2(a), the major strain field just before the onset of initial fracture was employed for the forming limits determination. Since a significant strain gradient is generated at the specimen thickness reduced area and the maximum strain was located at the specimen center, only one cross section passing through the specimen center and perpendicular to the crack was considered. As shown in Figure 2(b), the major strains along the cross section were fitted by an inverse parabolic curve ($f(x)=1/(ax^2+bx+c)$). The inner boundary of the fit window was determined by the maximum value of the second derivative of the major strains, while the width of the fit window was calculated by the function $W=10\times(1+\bar{\varepsilon}_2/\bar{\varepsilon}_1)$. The major limit strain was represented by the highest point of the inverse parabolic curve, and the minor limit strain was identified from the strain path at the corresponding major limit strain [17]. By adjusting the biaxial tensile ratios on the two cruciform specimens, the predicted FLC on the basis of CRIT1 is presented in Figure 6.

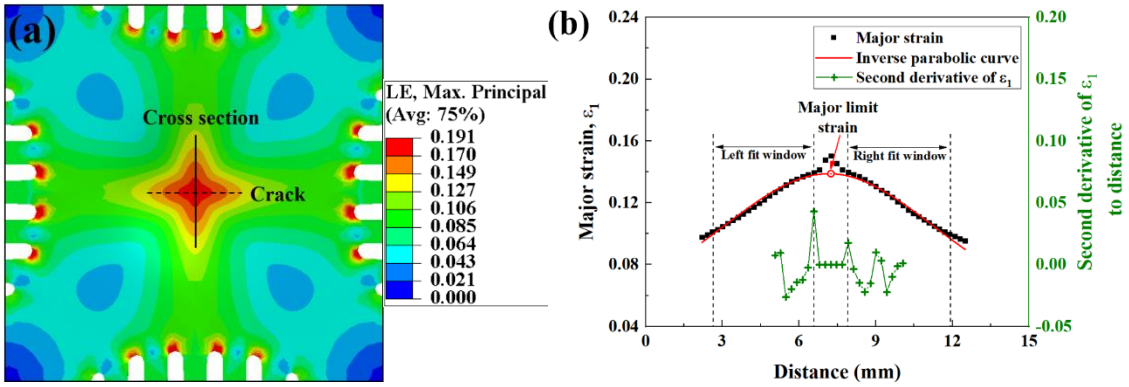


Figure 2. (a) The major strain field of specimen I under equi-biaxial loading condition, (b) determination of the major limit strain based on the CRIT1.

2.2.2. Thickness variation method (CRIT2). Once the localized necking occurs, material points within the necking area will show a significant difference in thickness variation rate compared to the points at the edge and outside of the necking area. Thickness variation method is based on this strain localisation, and the key is the identification of the center and edge of the necking area [10]. As shown in Figure 3, five points were created distant by 0.2mm along the direction perpendicular to the crack, starting from the center of the necking area. The thickness variation rates of the five points were analysed to identify the edge of the necking area and then determine the forming limits at necking. It can be seen, in Figure 3(c), that the curves of thickness variation rate for points P1, P2 and P3 decreased monotonically, while the slopes of the curves for P4 and P5 changed from negative to positive after the localized necking occurred. Thus, the edge of necking area was identified at P4, and the moment of localized necking was determined at the time when the slope of the thickness variation rate curve for P4 equal to zero. Subsequently, the forming limits at necking (point P1) can be identified according to the determined necking time. With the thickness variation method, CRIT2, the predicted FLC is presented in Figure 6.

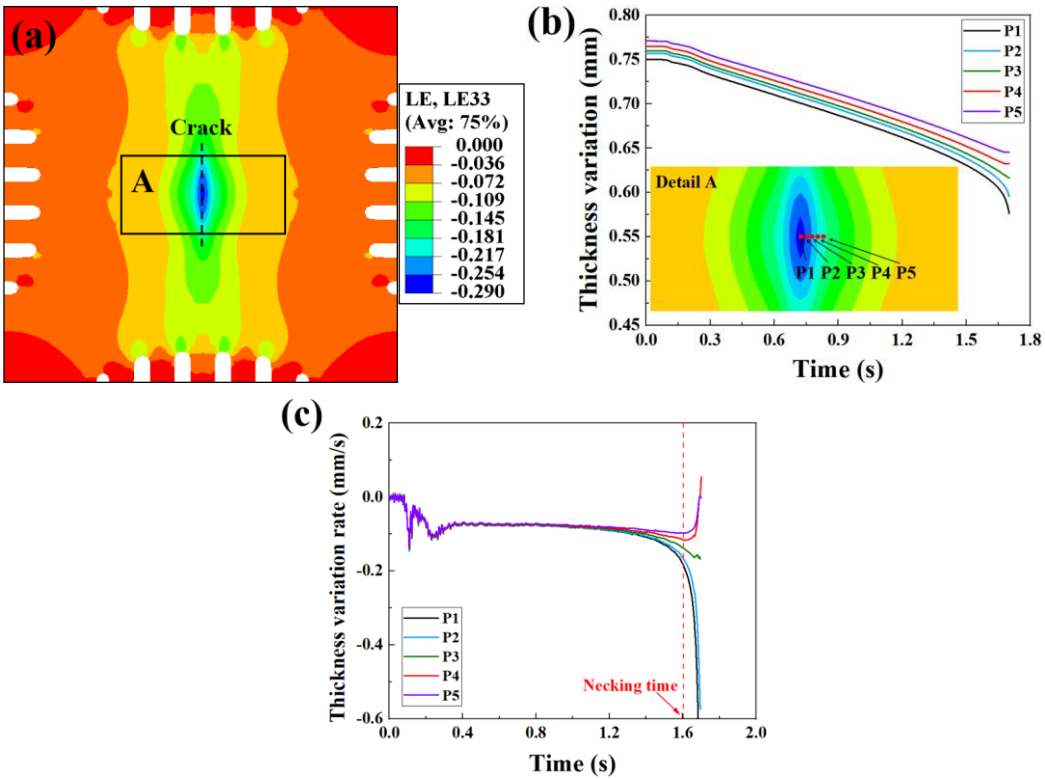
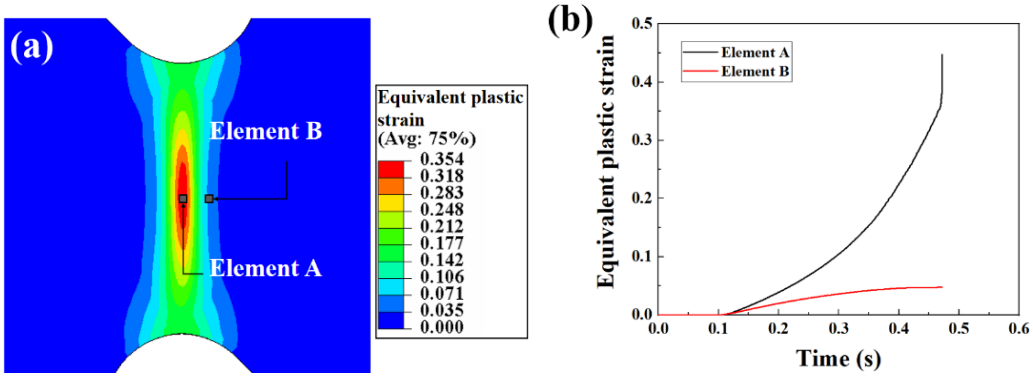


Figure 3. (a) The thickness strain field of specimen I under the biaxial tensile ratio of V_{L1}/V_{L2} = 1/0.4 (mm/s), (b) thickness variations of the five points, (c) determination of necking time based on the CRIT2.

2.2.3. Equivalent plastic strain increment ratio method (CRIT3). Figure 4 presents the application of CRIT3 to determine the forming limits at necking with specimen II under the plane strain condition. Two elements were selected on the surface of specimen II, where element A was at the center of the necking area and element B was outside the necking area at a distance of 1mm from element A. It can be seen in Figure 4(b), as entering the plastic domain, the equivalent plastic strain increase rate of element A was significantly higher than the one of element B. The ratio of the equivalent plastic strain increment between the two elements was calculated by the function (r=$\Delta\bar{\varepsilon}^{p}_{A}/\Delta\bar{\varepsilon}^{p}_{B}$), with a time interval of 0.025s. As presented in Figure 4(c), when the ratio reaches the critical value (in this work, the common value of 7 was selected), localized necking appears. Then, according to the found localized necking time, the forming limits at necking are given by the corresponding strain pairs. With the CRIT3, the predicted FLC is shown in Figure 6.



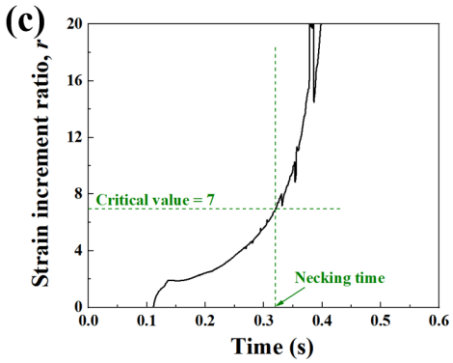


Figure 4. (a) Equivalent plastic strain field of specimen II under plane strain condition, (b) evolutions of the equivalent plastic strain in Elements A and B, (c) evolution of the equivalent strain increment ratio.

2.2.4. Spatio-temporal method (CRIT4). As shown in Figure 5(a), two rectangular zones (BZ and RZ) were defined on the surface of specimen II with the same symmetric line located at the center of necking area. The size of the BZ zone was 3.3×1.2 (mm) and the size of the RZ zone was 3.3×3 (mm). Since the localized necking induces an increase in the non-uniformity of the thickness strain distribution, more thickness strain is accumulated in the BZ zone, so that the ratio of the average thickness strain between the two zones develops nonlinearly. In this method, the localized necking is assumed to appear at the beginning of an increasing difference between the average thickness strain within the two zones. In figure 5(b), two straight lines were used to fit the uniform deformation stage and the final stage of the average thickness strain curve, respectively. The intersection point of the two fitted lines was recognized as the onset of localised necking. The FLC determined by CRIT4 is shown in Figure 6.

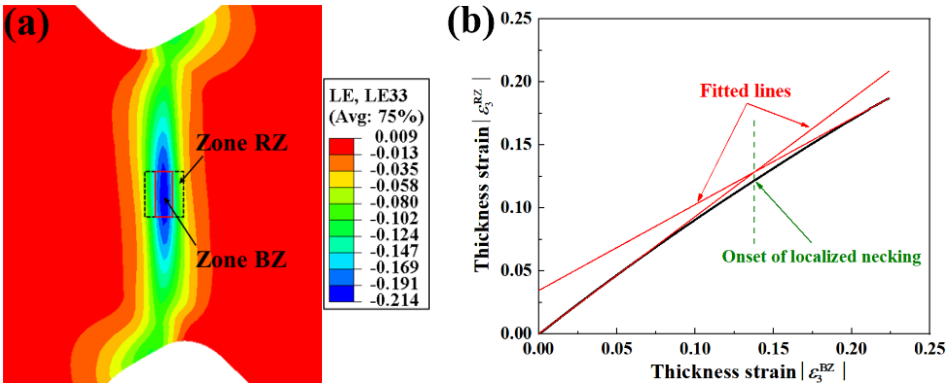


Figure 5. (a) Thickness strain field of specimen II under uniaxial tensile strain state, and selection of zones BZ and RZ. (b) Determination of onset of localised necking based on the CRIT4.

3. Comparison of the predicted FLCs and experimental validation

Figure 6(a) presents the FLCs determined by the four necking criteria. The right branch of the FLC was obtained from specimen I and the left branch from specimen II. The two specimens provided an overlapping area near the plane strain state, and the forming limits of the two specimens under the plane strain state were in good agreement. For the right branch, the forming limits determined by CRIT2 were slightly higher than the results of the other criteria. As CRIT2, CRIT3 and CRIT4 did not detect the occurrence of necking under the equi-biaxial loading condition, the fracture strain was used as the forming limits at necking. For the left branch, significant differences can be observed in the predicted FLCs, especially close to the uniaxial tension state. The reason for the difference might result from the large strain gradient due to the non-uniformed thickness reduction of specimen II.

Therefore, the numerical simulation of a conventional uniaxial tensile test was carried out. Then, the forming limits were determined by the four necking criteria respectively, and the results were utilized as reference values for the comparison. As shown in Figure 6(b), the major forming limit strains determined by CRIT3 and CRIT4 were close to the reference values, while the CRIT1 and CRIT2 provided significantly higher results than the reference values. It can be concluded that CRIT1 and CRIT2 are greatly influenced by the non-uniformed thickness reduction, and both criteria overestimate the forming limits in specimen II. In contrast, CRIT3 and CRIT4 are more stable and therefore more suitable for application to the specimen with non-uniformed thickness reduction.

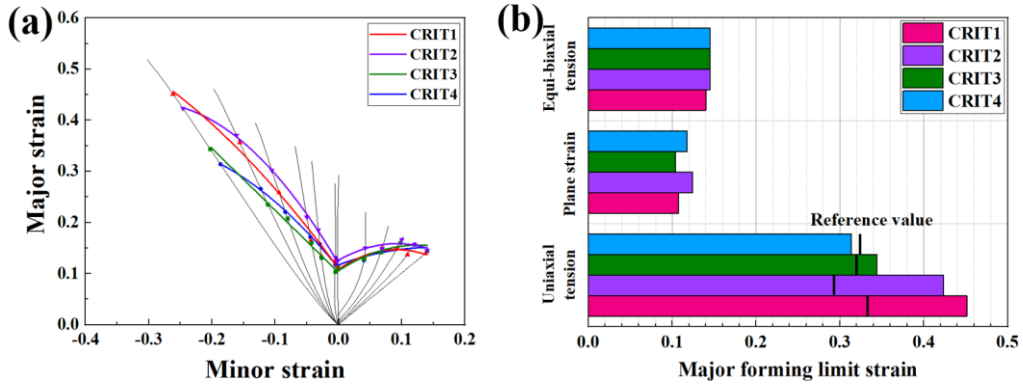


Figure 6. (a) The predicted FLCs of AA6061-T4 determined with different necking criteria, (b) the major forming limit strains for three representative strain states.

4. Conclusion

In this work, four existing necking criteria are applied and discussed for numerical procedure in order to evaluate their implementation for the specimens with non-uniformed thickness reduction. The results show that the non-uniformed thickness reduction causes CRIT1 and CRIT2 to overestimate the forming limits of the material. In contrast, CRIT3 and CRIT4 are more stable and therefore more suitable for the thickness reduced cruciform specimen. In addition, from an experimental point of view, the forming limit determination by CRIT1 relies on the best fit of an inverse parabolic curve; however the large strain gradient in the specimen with non-uniformed thickness reduction brings the challenge to the best fit. CRIT2 is greatly influenced by the noise in the strain measurement and therefore requires smoothing of the strain-time data. CRIT3 and CRIT4 are easy to use for experimental determinations of forming limits at necking. However, the critical value used in CRIT3 is usually empirical and lacks physical meaning. The width of the fitting window used to fit the straight lines in CRIT4 has a large influence on the results of the forming limits determination. A complete comparison between predictive and experimental results for all the strain paths will confirm the choice of the appropriate criterion.

References

[1] Keeler S P and Backhofen W A 1963 Plastic instability and fracture in sheet stretched over rigid punches. *Trans. Am. Soc. Met.* **56** 25–48
[2] BS EN ISO 12004, Metallic materials - Sheet and strip - Determination of forming limit curves Part 2: Determination of forming limit curves in the laboratory, 2008
[3] Min J, Stoughton T B, Carsley J E and Lin J 2016 Compensation for process-dependent effects in the determination of localized necking limits. *Int. J. Mech. Sci.* **117** 115-134
[4] Zhang R, Shi Z, Shao Z, Yardley V A and Lin J 2021 Biaxial test method for determination of FLCs and FFLCs for sheet metals: validation against standard Nakajima method. *Int. J. Mech. Sci.* **209** 106694
[5] Leotoing L, Guines D, Zidane I and Ragneau E 2013 Cruciform shape benefits for experimental and numerical evaluation of sheet metal formability. *J. Mater. Process. Tech.* **213** 856-863
[6] Zidane I, Guines D, Leotoing L and Ragneau E 2010 Development of an in-plane biaxial test

for forming limit curve (FLC) characterization of metallic sheets. *Meas. Sci. Technol.* **21**(5) 055701
[7] Song X, Leotoing L, Guines D and Ragneau E 2017 Characterization of forming limits at fracture with an optimized cruciform specimen: Application to DP600 steel sheets. *Int. J. Mech. Sci.* **126** 35-43
[8] Chu X, Wang Z, Chen C, Lin S and Leotoing L 2020 Experimental investigation of punch curvature influence in Nakazima test and numerical FLD prediction of AA5086. Ferroelectrics **565** 12-25
[9] Chu X, Leotoing L, Guines D and Ragneau E 2014 Temperature and strain rate influence on AA5086 Forming Limit Curves: experimental results and discussion on the validity of the MK model. *Int. J. Mech. Sci.* **78** 27-34
[10] Iquilio R A, Castro Cerda F M, Monsalve A, Guzman C F, Yanez S J, Pina J C, Vercruysse F, Petrov R H and Saavedra E I 2019 Novel experimental method to determine the limit strain by means of thickness variation. *Int. J. Mech. Sci.* **153-154** 208-218
[11] Marciniak Z, Kuczynski K 1967 Limit strains in the processes of stretch-forming sheet metal. *Int. J. Mech. Sci.* **9** 609-620
[12] Zhang C, Leotoing L, Zhao G, Guines D and Ragneau E 2011 A Comparative Study of Different Necking Criteria for Numerical and Experimental Prediction of FLCs. *J. Mater. Eng. Perform.* **20** 1036-1042
[13] Zhang R, Shi Z, Shao Z, Dean T A and Lin J 2021 A novel spatio-temporal method for determining necking and fracture strains of sheet metals. *Int. J. Mech. Sci.* **189** 105977
[14] Wang Z, Guines D, Chu X and Leotoing L 2022 Characterization of forming limits at fracture from shear to plane strain with a dedicated cruciform specimen. *Int. J. Mater. Form.* **15** 7
[15] Gurson A L 1977 Continuum theory of ductile rupture by void nucleation and growth: Part I - Yield criteria and flow rules for porous ductile media. *J. Eng. Mater. Technol.* **99** 2
[16] Yildiz R A and Yilmaz S 2020 Experimental Investigation of GTN model parameters of 6061 Al alloy. *Eur. J. Mech. A-Solid.* **83** 104040
[17] Noder J and Butcher C 2019 A comparative investigation into the influence of the constitutive model on the prediction of in-plane formability for Nakazima and Marciniak tests. *Int. J. Mech. Sci.* **163** 105138